

Label-free biomarker detection from whole blood

Eric Stern¹, Aleksandar Vacic², Nitin K. Rajan², Jason M. Criscione¹, Jason Park¹, Bojan R. Ilic³, David J. Mooney⁴, Mark A. Reed^{2,5*} and Tarek M. Fahmy^{1,6*}

Label-free nanosensors can detect disease markers to provide point-of-care diagnosis that is low-cost, rapid, specific and sensitive^{1–13}. However, detecting these biomarkers in physiological fluid samples is difficult because of problems such as biofouling and non-specific binding, and the resulting need to use purified buffers greatly reduces the clinical relevance of these sensors. Here, we overcome this limitation by using distinct components within the sensor to perform purification and detection. A microfluidic purification chip simultaneously captures multiple biomarkers from blood samples and releases them, after washing, into purified buffer for sensing by a silicon nanoribbon detector. This two-stage approach isolates the detector from the complex environment of whole blood, and reduces its minimum required sensitivity by effectively pre-concentrating the biomarkers. We show specific and quantitative detection of two model cancer antigens from a 10 μ l sample of whole blood in less than 20 min. This study marks the first use of label-free nanosensors with physiological solutions, positioning this technology for rapid translation to clinical settings.

Biomarkers have emerged as potentially important diagnostic tools for cancer and many other diseases. Continuing discoveries of such biomarkers and their aggregation into molecular signatures suggests that multiple biomarkers will be necessary to precisely define disease states. Thus, parallel detection of biomarker arrays is essential for translation from benchtop discovery to clinical validation. Such a technique would enable rapid, point-of-care (POC) applications requiring immediate diagnosis from a physiological sample. Critically, such a system must also be capable of detecting very low levels of aberrant genes and proteins, as many biomarkers are present at minute concentrations during early disease phases^{3–6}. Given these requirements, the use of conventional diagnostic assays^{5,6,14} has been a limiting factor. An approach that is based on rapid, label-free sensing technologies would be ideally suited for clinical applications^{6–13}.

Since their introduction in 2001 (ref. 7), label-free nanosensors have demonstrated great potential to serve as POC detectors capable of ultrasensitive, real-time, multiplexed detection of multiple biomolecular species^{6,8–13}. Despite their appeal, electronic nanosensors continue to be a challenge to implement, because fundamental limitations render them incapable of sensing molecules in complex, physiological solutions^{6,8–13}. Biofouling and non-specific binding readily degrade the minute active surface areas of such devices ($<0.1 \mu\text{m}^2$; ref. 15) and label-free sensing requires purified, precisely controlled buffers to enable measurements to be performed. In the case of nanowire field-effect transistor (FET) sensing, low salt ($<1 \text{ mM}$) buffers are required to prevent screening of the charge-based electronic signal^{12,16}.

To overcome these limitations we have developed a new in-line microfabricated device that operates upstream of the nanosensors to purify biomarkers of interest. This microfluidic purification chip (MPC) captures cancer biomarkers from physiological solutions and, after washing, releases the antigens¹⁷ into a pure buffer suitable for sensing. The chip design increases nanosensor specificity to that of conventional sandwich assay techniques, because it requires two antibodies to bind biomarkers for a positive signal to be produced¹⁸.

Figure 1 schematically illustrates the operation of the MPC. The avidin-functionalized chip¹⁹ (Fig. 1a) is treated with antibodies to any number of specific biomarkers conjugated to biotinylated, photocleavable crosslinkers containing a specific 19-mer DNA sequence (Fig. 2a)²⁰. The MPC geometry was chosen to optimize biomarker binding (Supplementary Fig. S1)¹⁴ and chips were fabricated from 4-inch silicon wafers in a one-step photolithographic process (Supplementary Fig. S2). Completed chips (Fig. 2b) were loaded into a custom-machined flow chamber (Fig. 2b, inset, and Supplementary Fig. S3), which enabled fluid handling and maintained a constant volume of 5 μ l in the system.

An example operation is illustrated in Fig. 1b–d. First, a blood sample flows through the chip (Fig. 1b) and the chip-bound antibodies bind specific soluble biomarkers, essentially purifying these molecules from whole blood. After this capture step, wash and sensing buffers are perfused through the device. Flow is then halted, and the sensing buffer-filled MPC is irradiated with ultraviolet (UV) light (Fig. 1c), resulting in cleavage of the photolabile group^{20–23} and release of the bound biomarker–antibody–DNA complexes. The UV photocleavage process was shown not to affect the immunoactivity of the biomarkers (Supplementary Fig. S4). The DNA component was critical for preliminary assay validation experiments (Fig. 2c). As shown in Fig. 1d, after a second valve switching step transfers MPC contents to the nanosensor chip, the complexes bind the secondary antibodies on the nanowire surfaces. The purification/sensing operation thus requires two specific antibody binding events for detection, a significant improvement in selectivity over previous label-free nanosensing schemes^{6–13}.

To demonstrate the effectiveness of the capture–release approach, we used a readily available fluorescently labelled antigen–antibody pair, fluorescently labelled chicken ovalbumin (OVA–FITC) and its antibody anti-OVA IgG. OVA–FITC was added to heparinized murine blood and flowed through an anti-OVA functionalized chip. After washing and flushing with sensing buffer, fluorescence imaging demonstrated specific OVA–FITC binding to chip-bound antibodies (Fig. 2d). A control chip, to which anti-prostate specific antigen (PSA) was bound, showed a negligible fluorescent signal (Fig. 2d, inset). After UV irradiation and subsequent flushing of the sensing reservoir with fresh buffer,

¹Department of Biomedical Engineering, School of Engineering and Applied Science, Yale University, New Haven, Connecticut 06511, USA, ²Department of Electrical Engineering, School of Engineering and Applied Science, Yale University, New Haven, Connecticut 06511, USA, ³Cornell Nanofabrication Facility, Cornell University, Ithaca, New York 14853, USA, ⁴Department of Bioengineering, School of Engineering and Applied Science, Harvard University, Cambridge, Massachusetts 02138, USA, ⁵Department of Applied Physics, School of Engineering and Applied Science, Yale University, New Haven, Connecticut 06511, USA, ⁶Department of Chemical Engineering, School of Engineering and Applied Science, Yale University, New Haven, Connecticut 06511, USA. *e-mail: mark.reed@yale.edu; tarek.fahmy@yale.edu

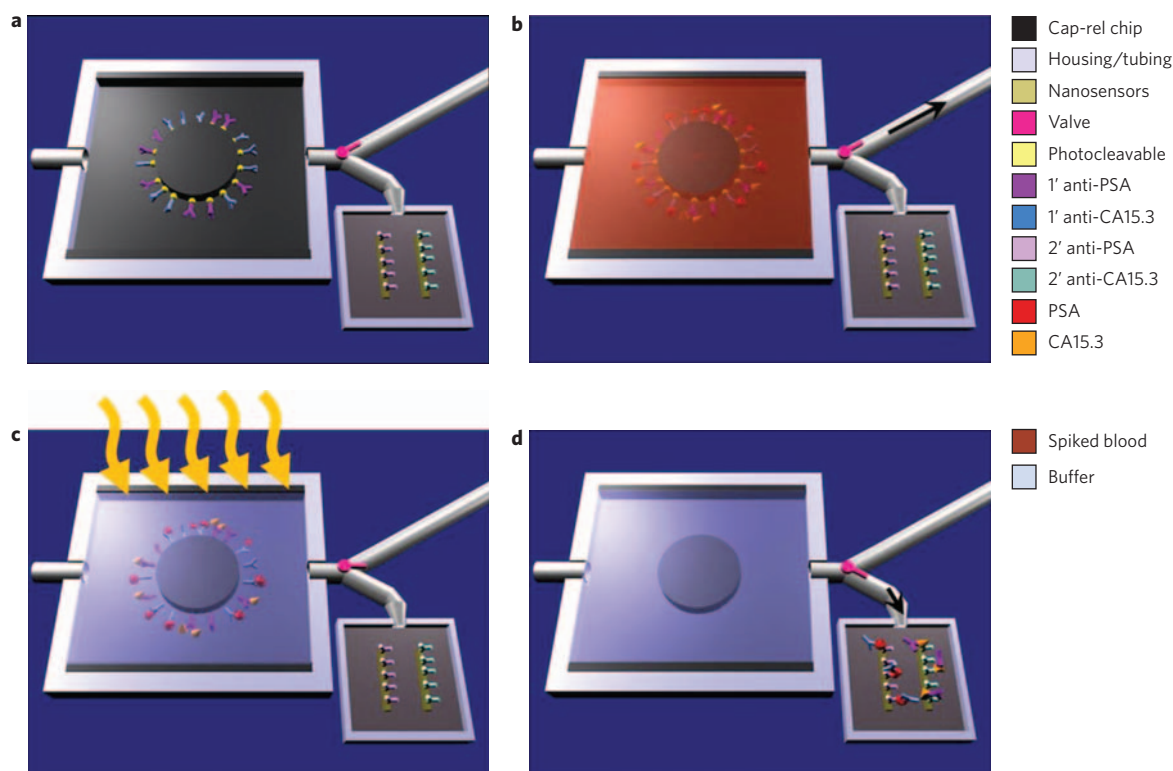


Figure 1 | Schematic of MPC operation. **a**, Primary antibodies to multiple biomarkers, here PSA and carbohydrate antigen 15.3 (CA15.3), are bound with a photocleavable crosslinker to the MPC. The chip is placed in a plastic housing and a valve (pink) directs fluid flow exiting the chip to either a waste receptacle or the nanosensor chip. **b**, Whole blood is injected into the chip with the valve set to the waste compartment (black arrow shows the direction of fluid flow) and, if present in the sample, biomarkers bind their cognate antibodies. **c**, Washing steps follow blood flow, and the chip volume (5 μl) is filled with sensing buffer before UV irradiation (orange arrows). During UV exposure, the photolabile crosslinker cleaves, releasing the antibody-antigen complexes into solution. **d**, The valve is set to the nanosensor reservoir (black arrow shows the direction of fluid flow) and the 5 μl volume is transferred, enabling label-free sensing to be performed to determine the presence of specific biomarkers.

the fluorescence signal from the anti-OVA chip was greatly diminished (Fig. 2d, inset).

To demonstrate the generality of the MPC technique, we used two model cancer antigens, PSA and carbohydrate antigen 15.3 (CA15.3), standard clinical markers for prostate^{24,25} and breast cancer^{26,27}, respectively. Successful capture and release of PSA and CA15.3 was verified with a modified enzyme-linked immunoassay (ELISA) technique (Fig. 2c)¹⁸, in which the first detection step consisted of the hybridization of a complementary, biotinylated 19-mer to the crosslinker DNA sequence. Six increasing concentrations of PSA and CA15.3 were added to heparinized rat blood and samples were flowed through MPCs functionalized with both anti-PSA and anti-CA15.3. The introduced concentrations spanned clinically relevant ranges^{24–27}. The data in Fig. 2e,f demonstrate a monotonic relationship between the concentration of biomarker introduced in whole blood and that released into pure sensing buffer. The absolute yields of these experiments are in agreement with modelling studies (Supplementary Fig. S1c). Biomarker capture by MPCs can be significantly increased by adjusting either the operation conditions, such as the flow rate into the device (modelled in Supplementary Fig. S1d), or the device dimensions.

A critical feature of this integrated approach is that the MPC-purified biomarker complex concentrations are well above those required for label-free, electronic detection. Although previous studies using nanowire sensors have demonstrated PSA detection levels as low as 0.9 pg ml^{-1} (refs 6,10), this exquisite sensitivity is not a critical factor for MPC-nanosensor operation. We thus chose to use ‘nanoribbons’, devices with nanoscale thicknesses

and microscale lateral dimensions²⁸, which are less sensitive but have significant fabrication and cost advantages. These devices, fabricated using conventional lithographic techniques, have been demonstrated to detect streptavidin in the 0.0318–53 ng ml^{-1} range²⁸, a sensitivity range ideally suited for MPC-purified cancer antigen detection. We fabricated 25-nm-thick devices according to a similar process (Supplementary Fig. S5)²⁸, but incorporated ohmic contacts to the devices. Device images are provided in Fig. 3a. Electrical characterization verified that this approach produced high-quality devices, with on/off ratios of $>10^6$ (Fig. 3b) and small hystereses between forward and reverse $I_{\text{DS}}(V_{\text{G}})$ sweeps (Fig. 3c), where I_{DS} is the drain–source current and V_{G} is the gate voltage. Surface functionalization did not compromise the device electrical characteristics (Supplementary Fig. S7), and solution gating ($V_{\text{G,SOLN}}$) demonstrated that $V_{\text{G}} = -5 \text{ V}$ was an optimal operating point for sensing studies (Fig. 3d).

As shown in Fig. 2 and detailed in the Supplementary Information, devices were functionalized either with anti-PSA or anti-CA15.3. Antibodies were immobilized to the sensor using N-hydroxysuccinimide (NHS)/1-ethyl-3-(3-dimethylaminopropyl) carbodiimide (EDC) chemistry. To verify that the signal from binding proteins would not be screened by the buffer solution, direct measurements of the amount of the signal that would be unscreened were carried out by varying buffer salt concentration¹⁶. This study indicated that $\sim 50\%$ of the signal was not screened by the buffer solution (see Supplementary Information).

We applied these devices to sensing the biomarkers from the MPC-purified whole blood samples. The normalized responses of these same devices to MPC-purified, antigen-spiked blood

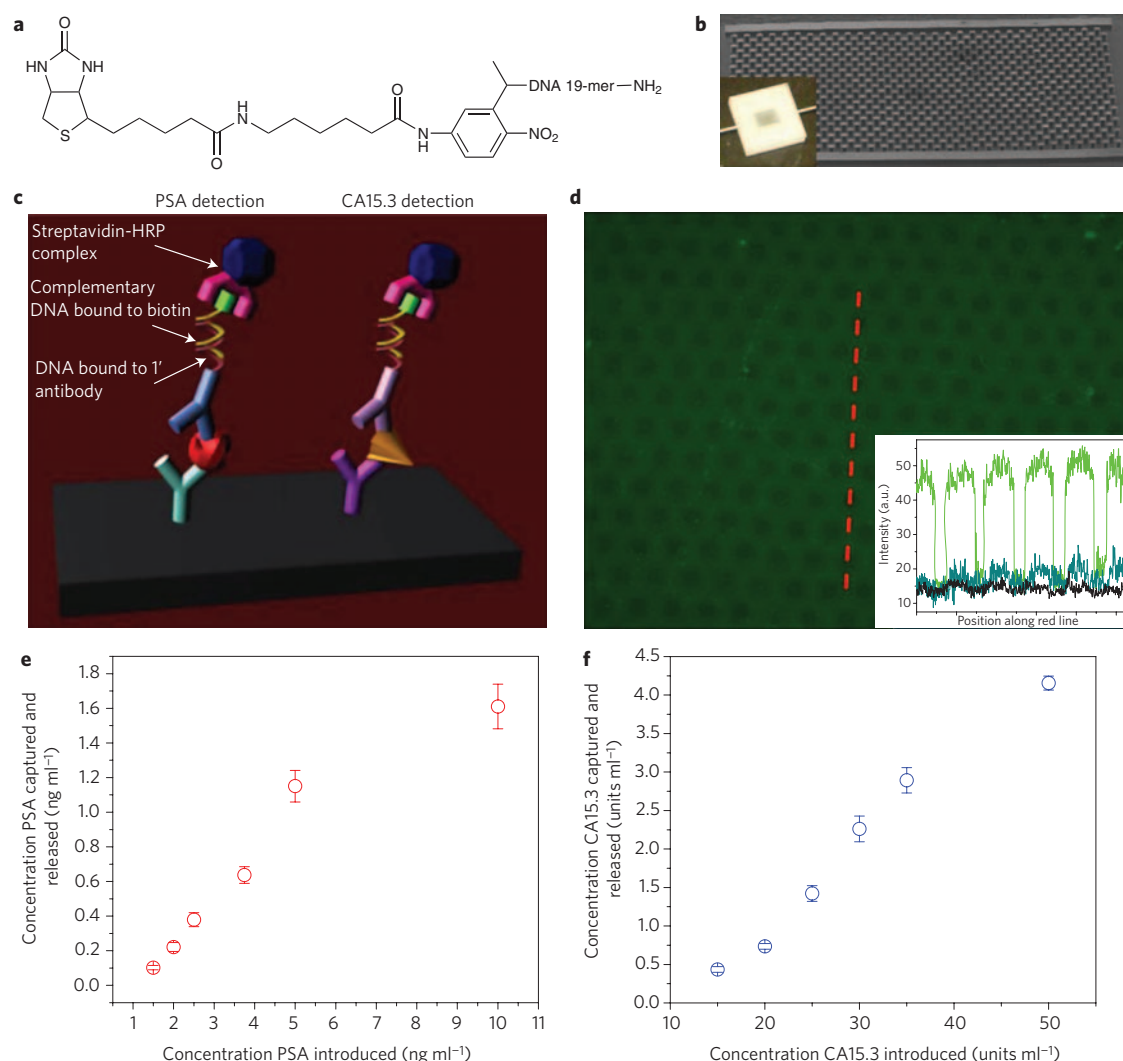


Figure 2 | MPC operation. **a**, Molecular structure of the photocleavable crosslinker. Primary antibody conjugation was performed with the amino group (right) and binding to chip-bound avidin occurred through the biotin group (left). **b**, Scanning electron micrograph of a representative ($w = 4 \text{ mm}$) \times ($l = 7 \text{ mm}$) \times ($h = 100 \text{ }\mu\text{m}$) MPC capture-release chip. The inset is an optical image of MPC operation during washing. **c**, Schematic representation of PSA and CA15.3 detection using a modified ELISA technique. **d**, Fluorescence optical micrograph of an anti-OVA functionalized MPC following OVA-FITC-spiked whole blood flow and washing. The inset plots the pixel intensity (grey value, determined by ImageJ) versus position for the red cut line (green data plot) and similar cut lines from images of post-UV irradiation and transfer (blue) and of an anti-PSA functionalized MPC following OVA-FITC-spiked blood flow and washing. The same exposure times were used for all images. **e**, **f**, Scatter plots showing the concentration of PSA (**e**) and CA15.3 (**f**) released from the MPC versus the concentration of PSA and CA15.3 introduced in whole blood, respectively. Each data point represents the average of three separate MPC runs, and error bars represent one standard deviation.

samples containing both 2.5 ng ml^{-1} PSA and 30 U ml^{-1} CA15.3 (as well as negative controls) are shown in Fig. 4a,b, respectively. After the injection transient noise subsided¹¹, device current levels were increased by antigen binding due to the negative charge conferred to the antigens by the basic sensing buffer. Similar signals were obtained with a PSA/CA15.3 spiked sensing buffer positive control, and no device response was observed with an unspiked, MPC-purified blood negative control. To reduce potential transient electrical signals upon injection, buffer salt concentrations of the functionalized devices and the MPC-purified samples were kept approximately the same. The positive signal was observed to increase linearly with time, following well-known ligand–receptor kinetics²⁹, in which initial rates at low relative analyte concentrations are directly proportional to species concentration³⁰. In fact, the asymptotic saturation value of the device response is weakly dependent on concentration for reversible reactions with a low dissociation constant²⁹, which is the case for the antigen–antibody

interactions. Thus, we focus on the initial kinetic reaction rates instead of endpoint detection³⁰.

Using these rates, a quantification of analyte concentrations (against a known) can be made, as shown in Fig. 4c,d. Whole blood samples spiked with 2 ng ml^{-1} PSA and 15 U ml^{-1} CA15.3 were MPC purified and sensed with anti-PSA and anti-CA15.3 functionalized devices. Using the slope of the normalized device temporal response, we find that the slope ratios of both the PSA and CA15.3 responses agree quite well with the initial spiked whole biomarker concentrations. For PSA, the slope ratio is 1.38, compared with a concentration ratio of 1.25; for CA15.3, the slope ratio is 1.94, compared with a concentration ratio of 2.0. It should be noted that this quantification occurs in the presence of another species, therefore also demonstrating selectivity (see Supplementary Information for further repeatability data).

The integration of a microfluidic purification step with label-free nanosensor detection represents a paradigm shift in label-free

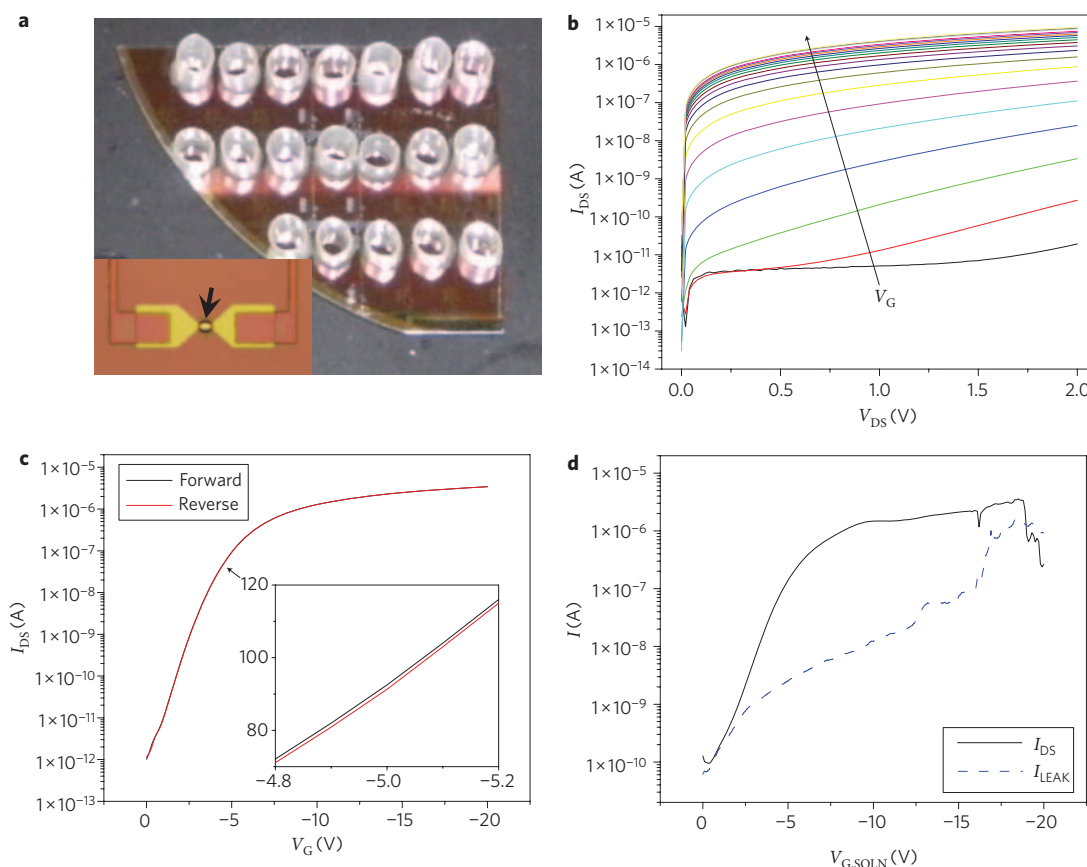


Figure 3 | Nanosensor electrical characteristics. **a**, Optical image of devices fitted with sensing reservoirs. The inset shows an optical micrograph of a complete device. Only the central region of the device (black arrow) is exposed to the solution. Metal leads contact the device source and drain and fan out to larger contacts (not shown). The 25-nm-thick silicon device appears yellow. **b**, $I_{DS}(V_{DS})$ plot with V_G varied from 0 to -20 V (black arrow shows the direction of increasing negative V_G) for a representative device illustrating p-type accumulation mode behaviour. V_{DS} , drain-source voltage. **c**, $I_{DS}(V_G)$ plot ($V_{DS}=1$ V) for the device used in **b**. The inset highlights I_{DS} (nA) around the operating point ($V_G=-5$ V). **d**, Plot demonstrating the effect of a varying solution gate voltage ($V_{G,SOLN}$) on device current (I_{DS} , black solid line) and device-to-solution leakage current (I_{LEAK} ; blue dashed line) for $V_{DS}=1$ V.

electronic sensing of biomolecules. The technique described here enables biomarker detection from whole blood or any other physiological fluid without the challenges associated with tailoring sensor operation for the medium of interest or engineering nanosensors that can withstand complex fluid media. Furthermore, the need for ultrasensitivity in electronic detection may not be essential with such an integrated platform because of its ability to pre-concentrate molecules of choice before sensing. The attractiveness of the method lies in its simplicity, speed and ability to simultaneously capture multiple biomarkers, enabling multiplexed, highly sensitive downstream detection with label-free sensors. This proof-of-principle demonstration of the non-integrated individual components should be easily integratable into a compact, self-contained system. Furthermore, the low cost of MPC purification renders this system capable of stand-alone use or use in tandem with more expensive sensing methodologies, such as rare circulating tumour cell detectors¹⁴, for more complex diagnoses. The portability and versatility of this method represents the crucial next step for label-free sensors and should position these and similar nascent sensing technologies for rapid molecular signature determinations.

Received 11 May 2009; accepted 15 October 2009;
published online 13 December 2009

References

- Sander, C. Genomic medicine and the future of health care. *Science* **287**, 1977–1978 (2000).
- Jemal, A. *et al.* Cancer statistics 2008. *CA Cancer J. Clin.* **58**, 71–96 (2008).
- Etzioni, R. *et al.* The case for early detection. *Nature Rev. Cancer* **3**, 243–252 (2003).
- Liang, S. & Chan, D. W. Enzymes and related proteins as cancer biomarkers: a proteomic approach. *Clin. Chim. Acta* **381**, 93–97 (2007).
- Fan, R. *et al.* Integrated barcode chips for rapid, multiplexed analysis of proteins in microliter quantities of blood. *Nature Biotechnol.* **26**, 1373–1378 (2008).
- Zheng, G., Patolsky, F., Cui, Y., Wang, W. U. & Lieber, C. M. Multiplexed electrical detection of cancer markers with nanowire sensor arrays. *Nature Biotechnol.* **23**, 1294–1301 (2005).
- Cui, Y., Wei, Q., Park, H. & Lieber, C. M. Nanowire nanosensors for highly sensitive and selective detection of biological and chemical species. *Science* **293**, 1289–1292 (2001).
- Jain, K. K. Nanotechnology in clinical laboratory diagnostics. *Clin. Chim. Acta* **358**, 37–54 (2005).
- Burg, Thomas T. P. *et al.* Weighing of biomolecules, single cells and single nanoparticles in fluid. *Nature* **446**, 1066–1069 (2007).
- Kim, A. *et al.* Ultrasensitive, label-free and real-time immunodetection using silicon field-effect transistors. *Appl. Phys. Lett.* **91**, 103901 (2007).
- Stern, E. *et al.* Label-free immunodetection with CMOS-compatible semiconducting nanowires. *Nature* **445**, 519–522 (2007).
- Stern, E., Vacic, A. & Reed, M. A. Semiconducting nanowire field-effect transistor biomolecular sensors. *IEEE Trans. Electron. Dev.* **55**, 3119–3130 (2008).
- Bunimovich, Y. L. *et al.* Quantitative real-time measurements of DNA hybridization with alkylated nonoxidized silicon nanowires in electrolyte solution. *J. Am. Chem. Soc.* **128**, 16323–16331 (2006).
- Nagrath, S. *et al.* Isolation of rare circulating tumor cells in cancer patients by microchip technology. *Nature* **450**, 1235–1239 (2007).
- Gupta, A. K. *et al.* Anomalous resonance in a nanomechanical biosensor. *Proc. Natl Acad. Sci. USA* **103**, 13362–13367 (2006).

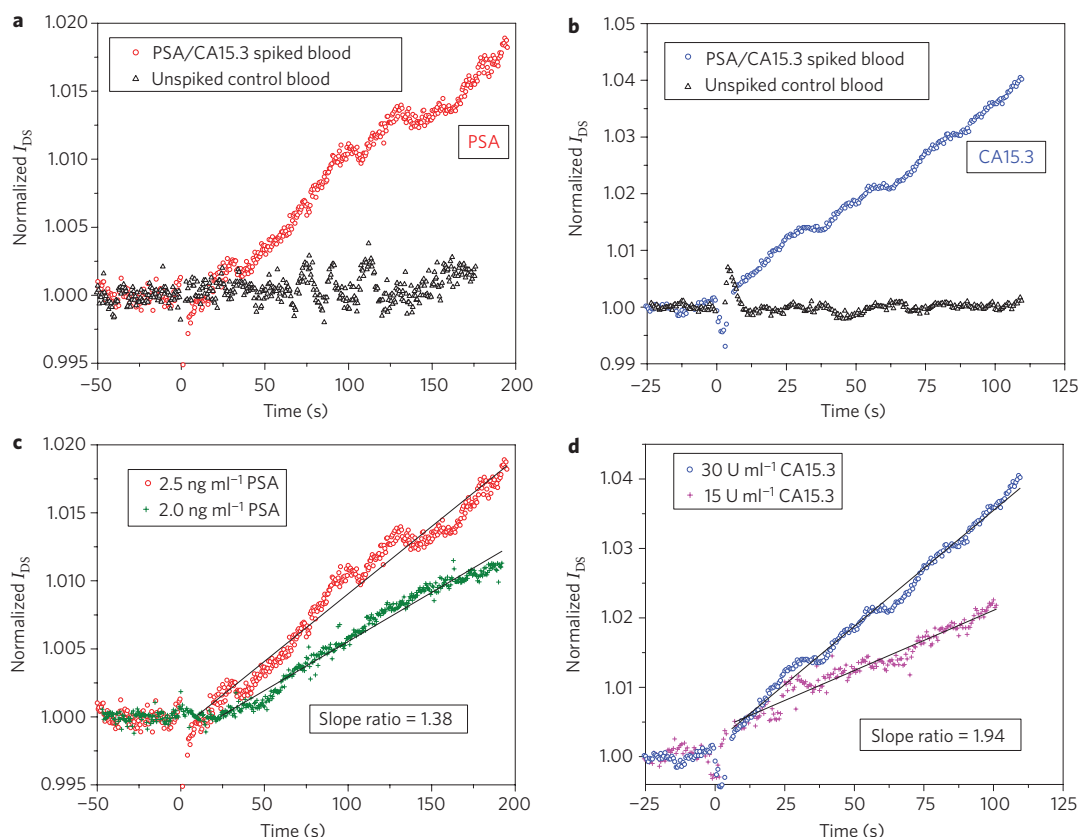


Figure 4 | Label-free sensing. All sensing measurements were performed at $V_{DS} = 1$ V and $V_G = -5$ V and all sample introductions occurred at $t = 0$. Normalizations were performed by dividing device currents by the pre-addition ($t < 0$) current level average. V_{DS} , drain-source voltage. **a**, Response of an anti-PSA functionalized sensor to a MPC-purified blood sample initially containing 2.5 ng ml⁻¹ PSA (and also 30 U ml⁻¹ CA15.3), or a control sample containing neither. **b**, Response of an anti-CA15.3 functionalized sensor to a MPC-purified blood sample initially containing 30 U ml⁻¹ CA15.3 (and also 2.5 ng ml⁻¹ PSA), or a control sample containing neither. **c,d**, Normalized response of two anti-PSA (**c**) and two anti-CA15.3 (**d**) functionalized devices to MPC-purified blood containing both PSA and CA15.3, with concentrations labelled. A least-squares fit is represented by a solid black line over the selected region (line endpoints). The ratio of the normalized slopes calibrates the ratio of concentrations.

16. Stern, E. *et al.* Importance of the Debye screening length on nanowire field effect transistor sensors. *Nano Lett.* **7**, 3405–3409 (2007).
17. Zhou, H., Ranish, J. A., Watts, J. D. & Aebersold, R. Quantitative proteome analysis by solid-phase isotope tagging and mass spectrometry. *Nature Biotechnol.* **20**, 512–515 (2002).
18. Templin, M. F., Stoll, D., Bachmann, J. & Joos, T. O. Protein microarrays and multiplexed sandwich immunoassays: what beats the beads? *Comb. Chem. High Through. Screen* **7**, 223–229 (2004).
19. Hermanson, G. T. *Bioconjugate Techniques* (Elsevier, 1996).
20. Bai, X., Kim, S., Li, Z., Turro, N. J. & Ju, J. Design and synthesis of a photocleavable biotinylated nucleotide for DNA analysis by mass spectrometry. *Nucleic Acids Res.* **32**, 535–541 (2004).
21. Handwerker, R. G. & Diamond, S. L. Biotinylated photocleavable polyethylenimine: capture and triggered release of nucleic acids from solid supports. *Bioconjug. Chem.* **18**, 717–723 (2007).
22. Senter, P. D. *et al.* Novel photocleavable protein crosslinking reagents and their use in the preparation of antibody–toxin conjugates. *Photochem. Photobiol.* **42**, 231–237 (1985).
23. Olejnik, J. *et al.* Photocleavable biotin derivatives—a versatile approach for the isolation of biomolecules. *Proc. Natl Acad. Sci. USA* **92**, 7590–7594 (1995).
24. Vickers, A. J., Savage, C., O'Brien, M. F. & Lilja, H. Systematic review of pretreatment prostate-specific antigen velocity and doubling time as predictors for prostate cancer. *J. Clin. Oncol.* **27**, 398–403 (2009).
25. Shariat, S. F., Scardino, P. T. & Lilja, H. Screening for prostate cancer: an update. *Can. J. Urol.* **15**, 4363–4374 (2008).
26. Rubach, M., Szymendera, J. J., Kaminska, J. & Kowalska, M. Serum CA 15.3, CEA and ESR patterns in breast cancer. *Int. J. Biol. Markers* **12**, 168–173 (1997).
27. Uehara, M. *et al.* Long-term prognostic study of carcinoembryonic antigen (CEA) and carbohydrate antigen 15-3 (CA 15-3) in breast cancer. *Int. J. Clin. Oncol.* **13**, 447–451 (2008).
28. Elfstrom, N., Karlstrom, A. E. & Linnros, J. Silicon nanoribbons for electrical detection of biomolecules. *Nano Lett.* **8**, 945–949 (2008).
29. Cantor, C. R. & Schimmel, P. R. *Biophysical Chemistry: Part III: The Behavior of Biological Macromolecules* (Freeman, 1980).
30. Homola, J. Present and future of surface plasmon resonance biosensors. *Anal. Bioanal. Chem.* **377**, 528–539 (2003).

Acknowledgements

The authors would like to thank J. Straight for many helpful discussions, M. Look and J. Bertram for blood samples, M. Power for device processing assistance, M. Saltzman for departmental support, and D. Stern and K. Milnamow for critical reading of the manuscript. The work was supported in part by the National Institute of Health (NIH) through grant no. R01EB008260 (M.A.R. and T.M.F.), Canadian Institute for Advanced Research (CIAR), and Army Research Office (ARO) (W911NF-08-1-0365). This work was performed in part at the Cornell Nanoscale Science and Technology Facility, a member of the National Nanotechnology Infrastructure Network that is supported by the National Science Foundation (NSF), and at the Yale Institute for Nanoscience and Quantum Engineering. This paper is dedicated to the memory of Alan R. Stern.

Author contributions

E.S. designed the MPC and performed all MPC experiments. E.S. and B.R.I. designed the MPC fabrication and performed MPC processing. E.S., A.V. and M.A.R. designed the nanosensor fabrication process and E.S., A.V. and B.R.I. performed nanosensor processing. D.J.M. assisted with MPC and nanosensor experimental design, and data analysis. E.S., A.V., N.K.R. and J.M.C. performed the sensing measurements. E.S., J.M.C. and J.P. prepared and analysed the protein samples. E.S., M.A.R. and T.M.F. wrote the manuscript and edited it, with contributions from all authors.

Additional information

The authors declare competing financial interests: details accompany the paper at www.nature.com/naturenanotechnology. Supplementary information accompanies this paper at www.nature.com/naturenanotechnology. Reprints and permission information is available online at <http://npg.nature.com/reprintsandpermissions/>. Correspondence and requests for materials should be addressed to M.A.R. and T.M.F.